ACS Photonics

pubs.acs.org/journal/apchd5

Article

Liquid Hydrogenation of Plasmonic Nanoantennas via Alcohol Deprotonation

Julian Karst,* Mario Hentschel, Florian Sterl, and Harald Giessen

Cite This: *ACS Photonics* 2021, 8, 1810−1816

Read Online

ACCESS | Metrics & More | Article Recommendations | Supporting Information

ABSTRACT: Yttrium is a metal whose optical properties are tunable by hydrogen incorporation. Commonly, this happens via exposure to hydrogen gas. Here, we demonstrate that the hydrogenation of yttrium is also possible via the deprotonation of alcoholic liquids. Palladium-covered yttrium is placed in an ethanol bath that causes the deprotonation of ethanol and the hydrogenation of yttrium to yttrium dihydride. Proof-of-concept is presented with a study on thin films, which is followed by tuning the optical properties of plasmonic nanoantennas. The liquid hydrogenation causes the plasmonic resonance to shift by more than 300 nm in the near-infrared spectral range. Consequently, we show that our plasmonic nanoantennas serve as a local nanooptical indicator for the deprotonation process. Our findings pave to road toward a (nano)optical investigation and detection of catalytic processes in liquids without the need of electrical, chemical, or electrochemical read-out.

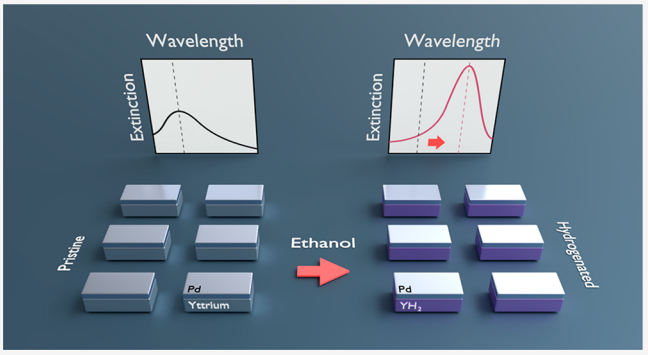

KEYWORDS: *metal hydrides, alcohol deprotonation, active plasmonics, catalysis, metal−insulator transitions, sensor*

Plasmonic nanophotonic systems fabricated from materials whose optical properties and material states are tunable upon external stimuli are of ever-increasing interest.[1] They allow the realization of plasmonic optical gas sensors,[2−4] plasmonic molecule detectors,[5−9] plasmonic displays,[10−15] tunable plasmonic metasurfaces,[16−22] and many more reversible and nonreversible applications. Especially plasmonic optical sensing platforms are an emerging field of interest as they allow, for example, to detect hydrogen (H_2) via an optical readout without further need of electronics in highly explosive environments.[23,24] Such sensors rely on the used plasmonic materials to be highly sensitive to a hydrogen exposure. Predestined and frequently used materials to show such unique properties are, for example, magnesium (Mg),[25−30] niobium (Nb),[31,32] yttrium (Y),[33,34] or palladium (Pd).[35−38] The latter is typically used as a catalyst to split hydrogen molecules at the Pd surface and to allow further diffusion of hydrogen atoms into the attached hydrogen-sensitive layers.

In this work we present a local nano-optical indicator that allows the detection of hydrogenation of yttrium nanoantennas via the deprotonation of alcohols assisted by a catalytic Pd cover. While common hydrogenation schemes of Y rely on hydrogen gas exposure, we show that, upon an exposure to liquid alcohols, such as ethanol or methanol, Y can be hydrogenated at room temperature and ambient pressures. This Pd-catalyzed deprotonation/oxidation of alcohols is known in the literature.[39−42] However, so far, it has not been possible to visualize such a deprotonation optically. After proving the concept in the visible (VIS) spectral range with Y−Pd thin films, we demonstrate a plasmonic nanoantenna resonance shift of several hundred nanometers in the near-infrared (NIR) and mid-infrared (MIR) spectral range after ethanol exposure. By varying the length of the plasmonic nanoantennas, we confirm excellent tunability and modulation of the plasmonic resonances as necessary for future wide-range applications. Our liquid hydrogenation method and nano-optical deprotonation indicator paves the way toward a purely optical local monitoring and detection of hydrogen-involving chemical processes in liquid environments without further need of electrical, chemical, or electrochemical read-out. It will be possible to optically and locally track chemical reactions where a local hydrogen indication is necessary, as for example during redox reactions in fuel cells to further improve their efficiency.

RESULTS AND DISCUSSION

The main concept of our liquid hydrogenation scheme is illustrated in Figure 1. The hybrid optical indicators consist of

Received: March 15, 2021
Published: May 12, 2021

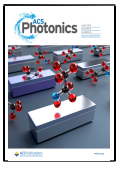

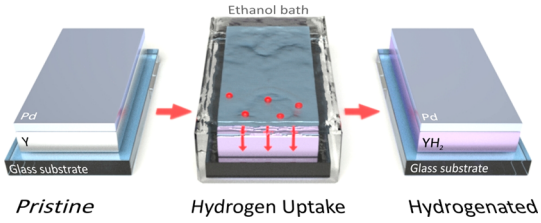

Figure 1. Concept of hydrogenation. The pristine optical indicators consist of a 50 nm yttrium (Y) layer covered with a 20 nm catalytic palladium (Pd) layer, as illustrated on the left. When placing such a sample in an ethanol bath (middle), the Pd layer causes the deprotonation of the ethanol and absorbs hydrogen (indicated by red spheres), which is then absorbed by the Y. After the immersion in the ethanol bath, the Y film has hydrogenated to a stable yttrium dihydride (YH_2) state, as indicated on the right.

stacked layers of yttrium (Y) and palladium (Pd) on glass substrates, as depicted on the left in Figure 1. This two-layered indicator is able to hydrogenate in an ethanol bath (Figure 1, middle), as the catalytic properties of Pd cause the deprotonation of ethanol and the hydrogen uptake of Pd and Y. As known from gasochromic hydrogenation experiments in which the samples are exposed to gaseous H_2 buffered in N_2 or synthetic air, Y is an excellent candidate to visualize its hydrogen uptake optically. Similarly, after the liquid hydrogenation, the optical properties of Y have changed dramatically, as stable yttrium dihydride (YH_2) has formed (Figure 1, right). This phase transition from metallic Y in hcp configuration to metallic YH_2 in fcc configuration comes with a strong increase in the electrical and optical conductivity. Consequently, YH_2 is the preferred metal to exhibit a plasmonic resonance, as we will show in the course of this work. Please note that the transition from Y to YH_2 is nonreversible at ambient pressures and room temperature. In contrast, Pd is expected to return to its pristine state as soon as the layered system is taken out of the ethanol bath, as we will also discuss in the course of the manuscript. Consequently, as mentioned, our new liquid hydrogenation method allows for a local optical indication and detection of chemical processes in liquids. We have to point out that, due to noncyclability, it is unlikely to be suited for reversible optical switching applications.

To prove our concept of liquid hydrogenation via the deprotonation of ethanol, we first study the change of the optical properties of Y–Pd thin films (50 nm Y + 20 nm Pd). The materials are evaporated subsequently via electron beam evaporation without breaking the vacuum. To keep the deposition conditions and thus the optical properties of the catalytic metals highly reproducible, we keep the deposition parameters (chamber pressure, deposition rate, film thicknesses, vacuumized material storage, etc.) identical for all samples shown in this work.[43] Figure 2 illustrates the change in the (a) reflectance and (b) transmittance spectrum in the VIS and NIR spectral range (500 to 900 nm). They are measured using a customized upright microscope spectroscopy system (NT&C NanoMicroSpec) referenced to an aluminum mirror (reflectance measurements) and to the bare substrate (transmittance measurements). The corresponding spectra of the film after immersion in ethanol are displayed in Figure 2a,b in red, the spectra for a gasochromic reference in blue, and the spectra of the pristine films in black. Numerical calculations of the reflectance and transmission spectra are plotted as dashed

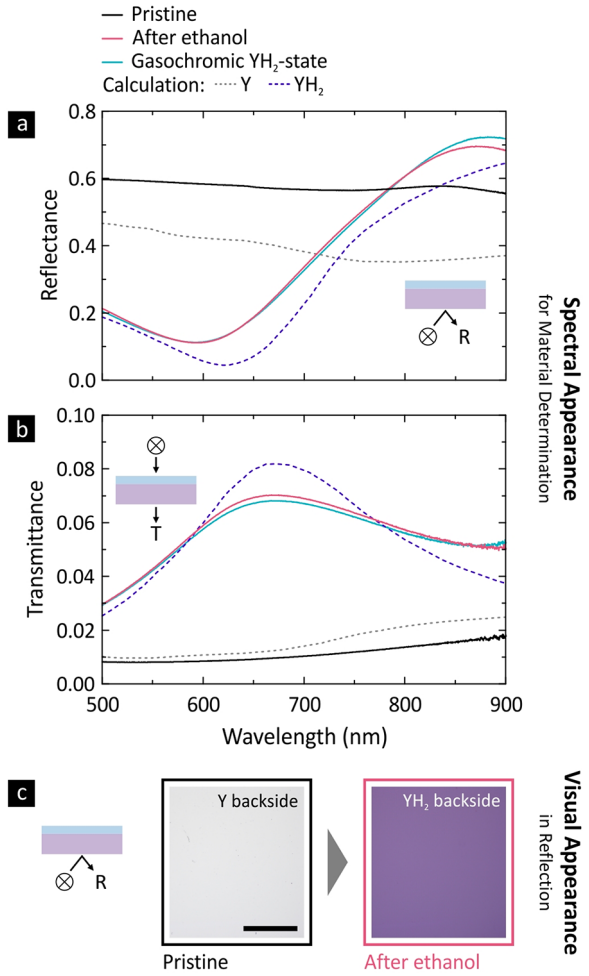

Figure 2. Material investigation via thin films: proof of concept. (a) Reflectance and (b) transmittance spectra of Y–Pd thin films in its pristine state (black solid lines), after an ethanol bath (red solid lines), in a gasochromic YH_2 state (blue solid lines), as well as calculated spectra for the pristine Y and hydrogenated YH_2 state (dashed lines). The spectra of the gasochromic YH_2 state and after ethanol agree very well, which implies also YH_2 material after the ethanol bath. We assume the Pd cap layer to return to its pristine state after the ethanol immersion and subsequent ambient air exposure, as validated by calculations (see Figure S1 in the Supporting Information). (c) Visual appearance of the backside of a pristine Y film and YH_2 film after ethanol. The images are taken with a reflection microscope. The scale bar is 1 mm and is valid for both images.

lines. The calculations are performed via a scattering matrix formalism.[44] The dielectric data of Y is taken from Weaver et al.,[45] and the data for YH_2 is taken from van Gogh et al.[46] We find that the optical properties change drastically upon ethanol and gas exposure. The reflectance of the thin films decreases from 0.6 to approximately 0.1 at 600 nm. Similarly, the transmittance increases by almost a factor of 7 from a value of approximately 0.01 to a value of 0.07. This characterization of the spectral appearance allows for the determination of the material state of Y after the liquid hydrogenation in an ethanol bath. Strikingly, the reflectance as well as the transmittance spectra of the ethanol state and the gasochromic YH_2 state are nearly identical. This proves that the immersion in ethanol leaves the film in the hydrogenated YH_2 state.

Furthermore, we assume the Pd cap layer to return to its pristine state after the ethanol immersion and subsequent

https://doi.org/10.1021/acsphotonics.1c00393
ACS Photonics 2021, 8, 1810–1816

ambient air exposure, as validated by calculations of different material stacks summarized in Figure S1 in the Supporting Information. In brief, we find that the calculated transmittance through a YH_2−PdH_x material stack where the cap layer is still hydrogenated overestimates the experimentally obtained values by a factor of 2. In contrast, we achieve a very good qualitative and quantitative agreement with the spectrum calculated for a YH_2−Pd combination, as it is depicted in Figure 2a,b.

Additionally, we performed the experiments using a wider set of solvents, in particular, of varying pK_a values. These results are shown in Figure S2 in the Supporting Information. Briefly, we compare an immersion of Y−Pd films in baths of ethanol, methanol, and acetone. We observe a very similar hydrogenation of Y for ethanol and methanol, whereas acetone (no alcohol) leaves the Y film unaffected. A detailed description of the gasochromic measurements can be found in Figure S3 of the Supporting Information.

Please note that Pd-capped yttrium is an ideal candidate to visualize this effect of liquid alcohol deprotonation. The reason lies with the very low hydrogen/proton partial pressure of only 10^{-30}−10^{-25} bar necessary for the transition from Y to YH_2 to start in a controlled environment without oxygen.[47] In contrast, the transition to the YH_3 state starts at comparably high partial pressures of 10^{-5}−10^{0} bar. Similarly, the phase transitions of pure Pd or other Pd-capped hydrogen-sensitive materials such as magnesium or niobium occur at similarly high hydrogen partial pressures, which are not reached by our liquid hydrogenation method. Please also note that even via common gas exposure a transition to full stoichiometric YH_3 cannot be reached. Typical experiments with Pd-capped Y stop at a hydrogen content YH_x of $x \approx 2.7$−2.9 (under very high pressure, $x = 2.99$ can be reached).[33]

Figure 2c shows the visual appearance of the backside of a pristine Y film (left) and of the same film after liquid hydrogenation in ethanol (right), taken in reflection (imaged through the glass substrate). The white balance is taken on the pristine Pd front side. We find, as expected, a silverish appearance of the pristine Y, whereas the film after the ethanol bath appears purple. As YH_2 becomes dielectric for $\lambda < 800$ nm this purple appearance is most likely due to a Fabry−Perot resonance in the YH_2 thin film which is tunable via the initial Y film thickness, as it known from previous work in literature.[48] Consequently, this resonance seems also to be the reason for the absorptive dip in the reflectance spectra of the hydrogenated YH_2 films in Figure 1a around $\lambda = 600$ nm.

For potential applications as optical indicator of local catalytic chemical processes it is important to understand the transition dynamics in more detail. Thus, we turn our attention to the temporal behavior of the transition from Y to YH_2. Figure 3a depicts the spectral change in reflection during the liquid hydrogenation upon ethanol exposure. For clarity we plot spectra every 8 min of ethanol exposure. The temporal spectral change clearly indicates the transition from the pristine Y state (black) to the hydrogenated YH_2 state (red) as the Fabry−Perot mode around $\lambda = 600$ nm becomes more and more pronounced, causing the reflectance to drop significantly. As seen in the time trace of the reflectance at $\lambda = 600$ nm in Figure 3b, the liquid hydrogenation of Y in the ethanol bath saturates after approximately 120 min (red curve). Further, acetone leaves the Y/Pd films unaffected as no hydrogen uptake via Pd is taking place (orange curve). A comparison to other alcohols is shown in Figure S3 in the Supporting Information. At this point we have to discuss the potential

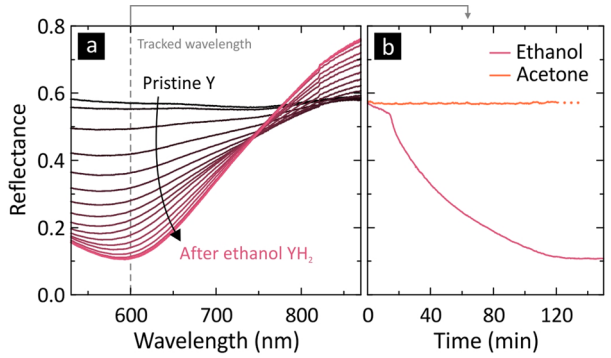

Figure 3. In situ temporal investigation of transition of Y thin films. (a) Reflectance spectra at every 8 min of the ethanol exposure. The transition from pristine Y (black) to YH_2 (red) is clearly observed. (b) Time trace of the change of the reflectance at a wavelength of 600 nm for ethanol exposure (red curve). For comparison, the time trace for acetone (orange) is depicted. Acetone leaves the pristine Y film unaffected.

reason for this liquid hydrogenation in ethanol. As mentioned above, we believe that the catalytic Pd layer causes a deprotonation of the alcohols, as it is known in case of Pd nanoclusters.[41,49] As the ability to deprotonate a solvent is directly related to its pK_a value, the hydrogenation speed should depend on the pK_a value of the solvent being used. The lower the pK_a value, the more likely is the deprotonation of the solvent, in turn speeding up the liquid hydrogenation. However, a lower pK_a value also implies a stronger acid which means that it becomes increasingly likely that highly reactive materials such as Y degrade.

For local detection of chemical reactions, it is necessary to transfer this hydrogenation concept to the micro- or nanometer scale. Our design of a local nano-optical indicator of the ethanol deprotonation is depicted in Figure 4a. We use plasmonic nanoantennas made from Y and Pd with a plasmonic resonance in the near-IR and mid-IR spectral ranges. These nanoparticles hydrogenate and change to YH_2 upon the liquid ethanol exposure and thus cause a large shift of the plasmonic resonance. The nanoparticles are fabricated via electron-beam lithography (EBL) and subsequent metal deposition via electron beam evaporation with a subsequent lift-off process. The pristine antennas have a length of 460 nm, a width of 190 nm, and a height of 70 nm (50 nm Y + 20 nm Pd cap). The periodicity of the antenna array is 700 nm in the x- and y-directions. An SEM image of the fabricated pristine array is depicted in the upper panel (black) of Figure 4b. The geometrical parameters lead to a somewhat weakly modulated plasmonic resonance of the pristine Y nanoantennas with a centroid wavelength at around 1390 nm, as shown in Figure 4a (black curve). The centroid wavelength defines the center of mass of the plasmonic resonance and is obtained via the algorithm from Dahlin et al.[50] The spectra are measured with a commercial Fourier transform infrared spectroscopy system (Bruker Vertex 80 with Hyperion 3000 microscope). This rather broad plasmonic resonance is caused by the low electrical conductivity of Y.[46,51] The actual existence of a resonance is mostly due to the 20 nm Pd cap. After the ethanol exposure we find the nanoantennas switched to the YH_2 state which, as shown above, causes a strong change in the optical properties. Consequently, the resonance of the nanoantennas shifts by more than 300 nm to a centroid wavelength of around 1700 nm, demonstrating excellent spectral separation between

https://doi.org/10.1021/acsphotonics.1c00393
ACS Photonics 2021, 8, 1810−1816

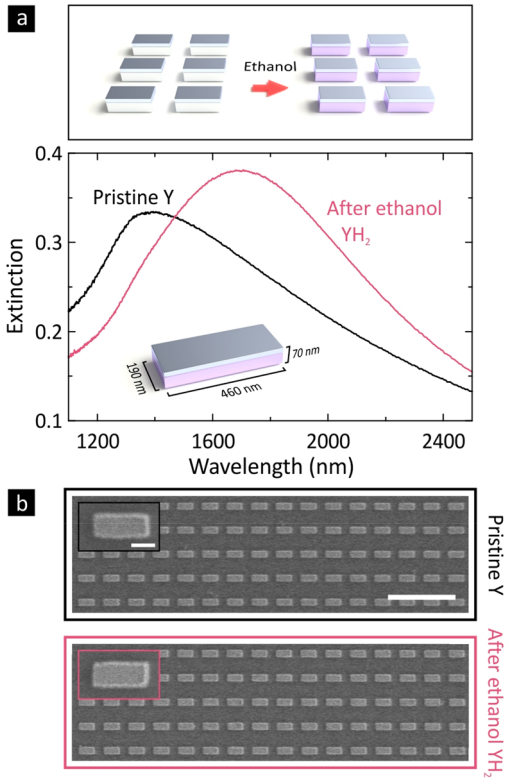

Figure 4. Nano-optical indicator for deprotonation process: hydrogenation of plasmonic nanoantennas. (a) Schematics of Y plasmonic nanoantennas hydrogenating in ethanol to metallic YH_2 (upper panel) as well as the corresponding change of the extinction spectra (lower panel). The pristine antennas have a length of 460 nm, a width of 190 nm, and a height of 70 nm (50 nm Y + 20 nm Pd). The periodicity of the array is 700 nm in the *x*- and *y*-directions. The plasmonic resonance for pristine Y (black curve) shows a peak wavelength at around 1390 nm and is somewhat weakly modulated. After the ethanol bath (red curve) the plasmonic resonance has red-shifted to a peak wavelength at around 1700 nm and is well modulated. (b) SEM images depicting the nanoantennas in its pristine state (black, upper panel) and after ethanol (red, lower panel). Although there has been a hydrogen uptake, no degradation or noticeable volume expansion is observable. The large scale bar is 2 μm. The small scale bar for the inset SEM images is 200 nm.

the pristine and hydrogenated state. Furthermore, the resonance is now well modulated as the conductivity of YH_2 is strongly increased in comparison to Y, which is caused by a change in the atomic and electronic structure upon hydrogen uptake.[52] Please note that both measurements in Figure 4a are taken when the sample is completely dry, once before (black curve) and once after (red curve) the ethanol exposure. This means that there is no liquid present during the measurement, which could have caused the red-shift of the plasmonic resonance due to a refractive index change of the surrounding medium. An SEM image of the YH_2 nanoantennas after ethanol exposure is shown in the lower panel (red) in Figure 4b. We find no deformation or noticeable expansion of the nanoantennas after hydrogenation. The reason lies with the comparably small volume expansion of only approximately 5% when Y changes to YH_2.[53] This conclusively demonstrates that the change and shift of the plasmonic resonance of our nano-optical indicator in Figure 4a is almost solely caused by the change in the electronic and consequently optical properties of the plasmonic nanoantennas upon ethanol deprotonation and hydrogen uptake.

In order to utilize yttrium nanoantennas as, for example, nano-optical plasmonic indicator, one has to be able to tune the plasmonic resonance over a wide spectral range. Thus, we vary the length of our plasmonic nanoantennas from L = 350 nm to L = 520 nm, while keeping the width (190 nm), the height (70 nm), and the periodicity (700 nm in *x*- and *y*-directions) constant. The spectral evolution of the corresponding plasmonic resonances is depicted in Figure 5 for YH_2 nanoantenna arrays which have been switched via (a) an ethanol bath and (b) gasochromically. Overall, we find perfect tunability of the plasmonic resonance and an excellent agreement between both experimental hydrogenation schemes. This underlines the exceptional power of our alcohol deprotonation technique to hydrogenate Y nanoantennas

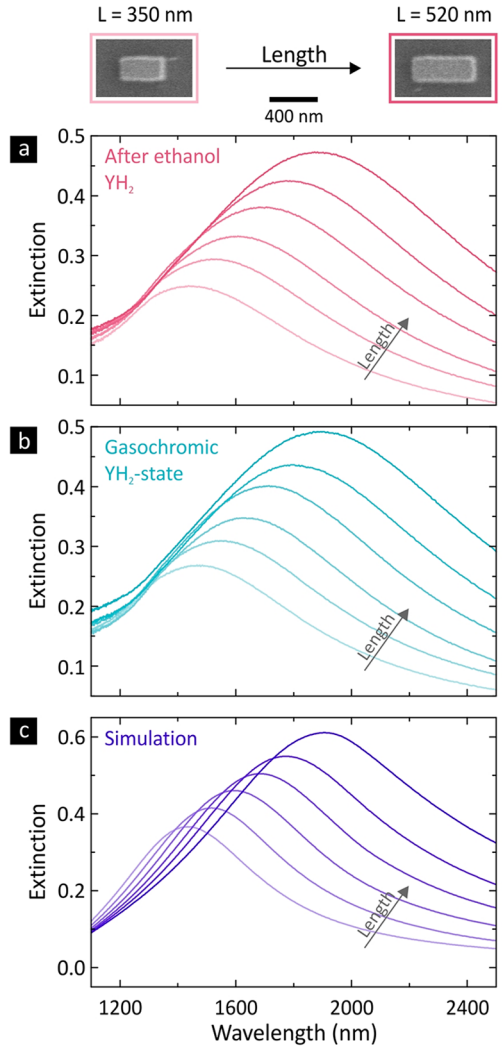

Figure 5. Plasmonic resonance tuning via ethanol, gasochromic comparison, and simulation of YH_2 nanoantennas. Extinction spectra of YH_2 plasmonic nanoantennas (a) after ethanol, (b) after gas exposure, and (c) simulated. The length of the antennas varies from 350 to 520 nm. The width is 190 nm and the height is 70 nm (50 nm YH_2 + 20 nm Pd). The cap layer for the simulations is in a Pd state as the samples are exposed to oxygen during the measurement and thus the PdH_x present during the ethanol/gas exposure is expected to dehydrogenate to Pd within seconds. In contrast, YH_2 remains stable at oxygen exposure at room temperature and ambient pressure.

https://doi.org/10.1021/acsphotonics.1c00393
ACS Photonics 2021, 8, 1810−1816

without the need for explosive hydrogen gases. Furthermore, Figure 5c illustrates the corresponding simulated plasmonic nanoantennas. The simulations are carried out with the frequency domain solver of CST Microwave Studio. The spectra of all pristine Y plasmonic nanoantenna spectra can be found in Figure S5 in the Supporting Information. As the nanoantennas in experiment form a native yttrium oxide (Y_2O_3) layer, we include a 3 nm thin Y_2O_3 shell in the simulations. Furthermore, the nanostructuring processes (PMMA masking and development, lift-off, etc.) can introduce small defects and impurities in the Y nanoantennas. To compensate for this degradation in the simulation, we increase the free electron damping in the respective dielectric function.[33] Consequently, we achieve very good agreement between experimentally measured and simulated YH_2 nanoantennas. In the experiments, the length tuning allows for a shift of the plasmonic resonance from approximately 1440 to 1890 nm. This closely matches the overall expected shift and absolute centroid position from the simulations.

CONCLUSION

In conclusion, we have demonstrated a novel method to hydrogenate yttrium films as well as yttrium nanoantennas in a liquid environment. We have carried out a proof-of-concept via alcohol hydrogenation of Y thin films to YH_2 and have shown excellent agreement with gasochromically switched films as well as with calculated optical responses. Our presented local nano-optical indicators for the deprotonation of alcohols consist of periodically arranged plasmonic nanoantennas realizing a resonance with great oscillator strength and wide tunability in the NIR and MIR spectral range. Upon alcohol exposure, the plasmonic resonance shifted by several hundreds of nanometers, leading to an excellent distinguishability between the pristine and hydrogenated state. Again, a comparison with gasochromically hydrogenated as well as simulated YH_2 nanoantennas revealed excellent agreement. Our findings have immediate implications in hydrogen-regulated optical and chemical systems and can lead to applications where a hydrogen detection and indication in liquids is required. A utilization of our liquid hydrogenation scheme in other metal hydride systems or hydrogen-sensitive materials such as metal–organic frameworks could, in the future, even allow for a reversibility of the liquid hydrogenation process. Volumetric detection limits of chemical reactions and catalytic processes in liquids can be even further pushed by using and investigating single plasmonic particles as local nanoprobes instead of the entire nanoantenna array. Furthermore, our work can be highly beneficial for a better understanding of chemical reactions in liquids as it paves the way toward accessing and visualizing the reaction optically and locally without the necessity of an additional electrical, chemical, or electrochemical readout.

ASSOCIATED CONTENT

Supporting Information

The Supporting Information is available free of charge at https://pubs.acs.org/doi/10.1021/acsphotonics.1c00393.

More detailed information about the palladium cap layer, the spectral and temporal influence of different alcohols/solvents on thin films and nanoantennas, as well as information on the gasochromic measurements (PDF)

AUTHOR INFORMATION

Corresponding Author

Julian Karst − *4th Physics Institute and Research Center SCoPE, University of Stuttgart, 70569 Stuttgart, Germany;* orcid.org/0000-0003-2422-8926; Phone: +49 711 685 64955; Email: j.karst@pi4.uni-stuttgart.de

Authors

Mario Hentschel − *4th Physics Institute and Research Center SCoPE, University of Stuttgart, 70569 Stuttgart, Germany;* orcid.org/0000-0002-6882-4183

Florian Sterl − *4th Physics Institute and Research Center SCoPE, University of Stuttgart, 70569 Stuttgart, Germany;* orcid.org/0000-0002-1025-6777

Harald Giessen − *4th Physics Institute and Research Center SCoPE, University of Stuttgart, 70569 Stuttgart, Germany*

Complete contact information is available at: https://pubs.acs.org/10.1021/acsphotonics.1c00393

Notes

The authors declare no competing financial interest.

ACKNOWLEDGMENTS

We acknowledge financial support from the European Research Council (ERC Advanced Grant Complexplas), Bundesministerium für Bildung und Forschung, and Deutsche Forschungsgemeinschaft (SPP1839 Tailored Disorder and SPP1391 Ultrafast Nanooptics). Furthermore, we would like to thank Prof. Dr. Ronald Griessen (Vrije Universiteit Amsterdam) for his valuable input and scientific discussions.

REFERENCES

(1) Wuttig, M.; Bhaskaran, H.; Taubner, T. Phase-Change Materials for Non-Volatile Photonic Applications. *Nat. Photonics* **2017**, *11* (8), 465−476.

(2) Nugroho, F. A. A.; Darmadi, I.; Cusinato, L.; Susarrey-Arce, A.; Schreuders, H.; Bannenberg, L. J.; da Silva Fanta, A. B.; Kadkhodazadeh, S.; Wagner, J. B.; Antosiewicz, T. J.; Hellman, A.; Zhdanov, V. P.; Dam, B.; Langhammer, C. Metal-polymer Hybrid Nanomaterials for Plasmonic Ultrafast Hydrogen Detection. *Nat. Mater.* **2019**, *18* (5), 489−495.

(3) Liu, N.; Tang, M. L.; Hentschel, M.; Giessen, H.; Alivisatos, A. P. Nanoantenna-Enhanced Gas Sensing in a Single Tailored Nanofocus. *Nat. Mater.* **2011**, *10* (8), 631−636.

(4) Tittl, A.; Mai, P.; Taubert, R.; Dregely, D.; Liu, N.; Giessen, H. Palladium-Based Plasmonic Perfect Absorber in the Visible Wavelength Range and Its Application to Hydrogen Sensing. *Nano Lett.* **2011**, *11* (10), 4366−4369.

(5) Rodrigo, D.; Limaj, O.; Janner, D.; Etezadi, D.; García De Abajo, F. J.; Pruneri, V.; Altug, H. Mid-Infrared Plasmonic Biosensing with Graphene. *Science* **2015**, *349* (6244), 165−168.

(6) Wu, C.; Khanikaev, A. B.; Adato, R.; Arju, N.; Yanik, A. A.; Altug, H.; Shvets, G. Fano-Resonant Asymmetric Metamaterials for Ultrasensitive Spectroscopy and Identification of Molecular Monolayers. *Nat. Mater.* **2012**, *11* (1), 69−75.

(7) Neubrech, F.; Pucci, A.; Cornelius, T. W.; Karim, S.; García-Etxarri, A.; Aizpurua, J. Resonant Plasmonic and Vibrational Coupling in a Tailored Nanoantenna for Infrared Detection. *Phys. Rev. Lett.* **2008**, *101* (15), 2−5.

(8) Kühner, L.; Semenyshyn, R.; Hentschel, M.; Neubrech, F.; Tarín, C.; Giessen, H. Vibrational Sensing Using Infrared Nanoantennas: Toward the Noninvasive Quantitation of Physiological Levels of Glucose and Fructose. *ACS Sens.* **2019**, *4* (8), 1973−1979.

(9) Semenyshyn, R.; Hentschel, M.; Stanglmair, C.; Teutsch, T.; Tarin, C.; Pacholski, C.; Giessen, H.; Neubrech, F. In Vitro

Monitoring Conformational Changes of Polypeptide Monolayers Using Infrared Plasmonic Nanoantennas. *Nano Lett.* **2019**, *19* (1), 1−7.
(10) Duan, X.; Kamin, S.; Liu, N. Dynamic Plasmonic Colour Display. *Nat. Commun.* **2017**, *8* (1), 14606.
(11) Joo, W.-J.; Kyoung, J.; Esfandyarpour, M.; Lee, S.-H.; Koo, H.; Song, S.; Kwon, Y.-N.; Song, S. H.; Bae, J. C.; Jo, A.; Kwon, M.; Han, S. H.; Kim, S.-H.; Hwang, S.; Brongersma, M. L. Metasurface-Driven OLED Displays beyond 10,000 Pixels per Inch. *Science* **2020**, *370* (6515), 459−463.
(12) Li, J.; Yu, P.; Zhang, S.; Liu, N. Electrically-Controlled Digital Metasurface Device for Light Projection Displays. *Nat. Commun.* **2020**, *11* (1), 3574.
(13) Franklin, D.; Frank, R.; Wu, S. T.; Chanda, D. Actively Addressed Single Pixel Full-Colour Plasmonic Display. *Nat. Commun.* **2017**, *8* (1), 1−10.
(14) Duan, X.; Liu, N. Scanning Plasmonic Color Display. *ACS Nano* **2018**, *12* (8), 8817−8823.
(15) Neubrech, F.; Duan, X.; Liu, N. Dynamic Plasmonic Color Generation Enabled by Functional Materials. *Sci. Adv.* **2020**, *6* (36), eabc2709.
(16) Yin, X.; Steinle, T.; Huang, L.; Taubner, T.; Wuttig, M.; Zentgraf, T.; Giessen, H. Beam Switching and Bifocal Zoom Lensing Using Active Plasmonic Metasurfaces. *Light: Sci. Appl.* **2017**, *6* (7), No. e17016.
(17) Yu, P.; Li, J.; Li, X.; Schutz, G.; Hirscher, M.; Zhang, S.; Liu, N. Generation of Switchable Singular Beams with Dynamic Metasurfaces. *ACS Nano* **2019**, *13* (6), 7100−7106.
(18) Ratzsch, J.; Karst, J.; Fu, J.; Ubl, M.; Pohl, T.; Sterl, F.; Malacrida, C.; Wieland, M.; Reineke, B.; Zentgraf, T.; Ludwigs, S.; Hentschel, M.; Giessen, H. Electrically Switchable Metasurface for Beam Steering Using PEDOT Polymers. *J. Opt.* **2020**, *22* (12), 124001.
(19) Park, J.; Jeong, B. G.; Kim, S. Il; Lee, D.; Kim, J.; Shin, C.; Lee, C. B.; Otsuka, T.; Kyoung, J.; Kim, S.; Yang, K.-Y.; Park, Y.-Y.; Lee, J.; Hwang, I.; Jang, J.; Song, S. H.; Brongersma, M. L.; Ha, K.; Hwang, S.-W.; Choo, H.; Choi, B. L. All-Solid-State Spatial Light Modulator with Independent Phase and Amplitude Control for Three-Dimensional LiDAR Applications. *Nat. Nanotechnol.* **2021**, *16* (1), 69−76.
(20) Shaltout, A. M.; Shalaev, V. M.; Brongersma, M. L. Spatiotemporal Light Control with Active Metasurfaces. *Science* **2019**, *364* (6441), No. eaat3100.
(21) Park, J.; Kim, S. J.; Landreman, P.; Brongersma, M. L. An Over-Coupled Phase-Change Metasurface for Efficient Reflection Phase Modulation. *Adv. Opt. Mater.* **2020**, *8* (20), 2000745.
(22) Park, J.; Kang, J. H.; Kim, S. J.; Liu, X.; Brongersma, M. L. Dynamic Reflection Phase and Polarization Control in Metasurfaces. *Nano Lett.* **2017**, *17* (1), 407−413.
(23) Herkert, E.; Sterl, F.; Strohfeldt, N.; Walter, R.; Giessen, H. Low-Cost Hydrogen Sensor in the Ppm Range with Purely Optical Readout. *ACS Sens.* **2020**, *5* (4), 978−983.
(24) Miliutina, E.; Guselnikova, O.; Chufistova, S.; Kolska, Z.; Elashnikov, R.; Burtsev, V.; Postnikov, P.; Svorcik, V.; Lyutakov, O. Fast and All-Optical Hydrogen Sensor Based on Gold-Coated Optical Fiber Functionalized with Metal-Organic Framework Layer. *ACS Sens.* **2019**, *4* (12), 3133−3140.
(25) Karst, J.; Sterl, F.; Linnenbank, H.; Weiss, T.; Hentschel, M.; Giessen, H. Watching In-Situ the Hydrogen Diffusion Dynamics in Magnesium on the Nanoscale. *Sci. Adv.* **2020**, *6* (19), No. eaaz0566.
(26) Sterl, F.; Strohfeldt, N.; Walter, R.; Griessen, R.; Tittl, A.; Giessen, H. Magnesium as Novel Material for Active Plasmonics in the Visible Wavelength Range. *Nano Lett.* **2015**, *15* (12), 7949−7955.
(27) Baldi, A.; Mooij, L.; Palmisano, V.; Schreuders, H.; Krishnan, G.; Kooi, B. J.; Dam, B.; Griessen, R. Elastic versus Alloying Effects in Mg-Based Hydride Films. *Phys. Rev. Lett.* **2018**, *121* (25), 255503.
(28) Drechsler, V.; Krauth, J.; Karst, J.; Giessen, H.; Hentschel, M. Switchable Optical Nonlinearity at the Metal to Insulator Transition in Magnesium Thin Films. *ACS Photonics* **2020**, *7* (6), 1560−1568.
(29) Uchida, H. T.; Wagner, S.; Hamm, M.; Kürschner, J.; Kirchheim, R.; Hjörvarsson, B.; Pundt, A. Absorption Kinetics and Hydride Formation in Magnesium Films: Effect of Driving Force Revisited. *Acta Mater.* **2015**, *85*, 279−289.
(30) Hamm, M.; Bongers, M. D.; Roddatis, V.; Dietrich, S.; Lang, K.-H.; Pundt, A. In Situ Observation of Hydride Nucleation and Selective Growth in Magnesium Thin-Films with Environmental Transmission Electron Microscopy. *Int. J. Hydrogen Energy* **2019**, *44* (60), 32112−32123.
(31) Bagheri, S.; Strohfeldt, N.; Ubl, M.; Berrier, A.; Merker, M.; Richter, G.; Siegel, M.; Giessen, H. Niobium as Alternative Material for Refractory and Active Plasmonics. *ACS Photonics* **2018**, *5* (8), 3298−3304.
(32) Wagner, S.; Klose, P.; Burlaka, V.; Nörthemann, K.; Hamm, M.; Pundt, A. Structural Phase Transitions in Niobium Hydrogen Thin Films: Mechanical Stress, Phase Equilibria and Critical Temperatures. *ChemPhysChem* **2019**, *20* (14), 1890−1904.
(33) Strohfeldt, N.; Tittl, A.; Schäferling, M.; Neubrech, F.; Kreibig, U.; Griessen, R.; Giessen, H. Yttrium Hydride Nanoantennas for Active Plasmonics. *Nano Lett.* **2014**, *14* (3), 1140−1147.
(34) Huiberts, J. N.; Griessen, R.; Rector, J. H.; Wijngaarden, R. J.; Dekker, J. P.; De Groot, D. G.; Koeman, N. J. Yttrium and Lanthanum Hydride Films with Switchable Optical Properties. *Nature* **1996**, *380* (6571), 231−234.
(35) Narayan, T. C.; Hayee, F.; Baldi, A.; Leen Koh, A.; Sinclair, R.; Dionne, J. A. Direct Visualization of Hydrogen Absorption Dynamics in Individual Palladium Nanoparticles. *Nat. Commun.* **2017**, *8*, 1−8.
(36) Baldi, A.; Narayan, T. C.; Koh, A. L.; Dionne, J. A. In Situ Detection of Hydrogen-Induced Phase Transitions in Individual Palladium Nanocrystals. *Nat. Mater.* **2014**, *13* (12), 1143−1148.
(37) Ulvestad, A.; Yau, A. The Self-Healing of Defects Induced by the Hydriding Phase Transformation in Palladium Nanoparticles. *Nat. Commun.* **2017**, *8* (1), 1−6.
(38) Yau, A.; Harder, R. J.; Kanan, M. W.; Ulvestad, A. Imaging the Hydrogen Absorption Dynamics of Individual Grains in Polycrystalline Palladium Thin Films in 3D. *ACS Nano* **2017**, *11* (11), 10945−10954.
(39) Besson, M.; Gallezot, P. Selective Oxidation of Alcohols and Aldehydes on Metal Catalysts. *Catal. Today* **2000**, *57* (1−2), 127−141.
(40) Crabtree, R. H. Homogeneous Transition Metal Catalysis of Acceptorless Dehydrogenative Alcohol Oxidation: Applications in Hydrogen Storage and to Heterocycle Synthesis. *Chem. Rev.* **2017**, *117* (13), 9228−9246.
(41) Muzart, J. Palladium-Catalysed Oxidation of Primary and Secondary Alcohols. *Tetrahedron* **2003**, *59* (31), 5789−5816.
(42) Kluytmans, J. H. J.; Markusse, A. P.; Kuster, B. F. M.; Marin, G. B.; Schouten, J. C. Engineering Aspects of the Aqueous Noble Metal Catalysed Alcohol Oxidation. *Catal. Today* **2000**, *57* (1−2), 143−155.
(43) Karst, J.; Hentschel, M.; Sterl, F.; Linnenbank, H.; Ubl, M.; Giessen, H. Optimizing Magnesium Thin Films for Optical Switching Applications: Rules and Recipes. *Opt. Mater. Express* **2020**, *10* (6), 1346.
(44) Weiss, T.; Gippius, N. A.; Tikhodeev, S. G.; Granet, G.; Giessen, H. Efficient Calculation of the Optical Properties of Stacked Metamaterials with a Fourier Modal Method. *J. Opt. A: Pure Appl. Opt.* **2009**, *11* (11), 114019.
(45) Weaver, J. H.; Olson, C. G. Optical Absorption of Hcp Yttrium. *Phys. Rev. B* **1977**, *15* (2), 590−594.
(46) van Gogh, A. T. M.; Nagengast, D. G.; Kooij, E. S.; Koeman, N. J.; Rector, J. H.; Griessen, R.; Flipse, C. F. J.; Smeets, R. J. J. G. A. M. Structural, Electrical, and Optical Properties of La1-zYzHxswitchable Mirrors. *Phys. Rev. B: Condens. Matter Mater. Phys.* **2001**, *63* (19), 1−21.
(47) Kooij, E. S.; van Gogh, A. T. M.; Griessen, R. In Situ Resistivity Measurements and Optical Transmission and Reflection Spectroscopy of Electrochemically Loaded Switchable YH x Films. *J. Electrochem. Soc.* **1999**, *146* (8), 2990−2994.

https://doi.org/10.1021/acsphotonics.1c00393
ACS Photonics 2021, 8, 1810−1816

(48) Ngene, P.; Radeva, T.; Slaman, M.; Westerwaal, R. J.; Schreuders, H.; Dam, B. Seeing Hydrogen in Colors: Low-Cost and Highly Sensitive Eye Readable Hydrogen Detectors. *Adv. Funct. Mater.* **2014**, *24* (16), 2374−2382.
(49) Xin, P.; Li, J.; Xiong, Y.; Wu, X.; Dong, J.; Chen, W.; Wang, Y.; Gu, L.; Luo, J.; Rong, H.; Chen, C.; Peng, Q.; Wang, D.; Li, Y. Revealing the Active Species for Aerobic Alcohol Oxidation by Using Uniform Supported Palladium Catalysts. *Angew. Chem.* **2018**, *130* (17), 4732−4736.
(50) Dahlin, A. B.; Tegenfeldt, J. O.; Höök, F. Improving the Instrumental Resolution of Sensors Based on Localized Surface Plasmon Resonance Interfacial Refractive Index of Nanoscale Noble Metal Generic Data Analysis Algorithms and a Simple Experimen-Comparable to That of State-of-the Art SPR Systems. *Anal. Chem.* **2006**, *78* (13), 4416−4423.
(51) Bour, G.; Reinholdt, A.; Stepanov, A.; Keutgen, C.; Kreibig, U. Optical and Electrical Properties of Hydrogenated Yttrium Nanoparticles. *Eur. Phys. J. D* **2001**, *16* (1), 219−223.
(52) Stepanov, A. L.; Bour, G.; Gartz, M.; Osin, Y. N.; Reinholdt, A.; Kreibig, U. Synthesis of Yttrium Clusters. *Vacuum* **2001**, *64* (1), 9−14.
(53) Dornheim, M.; Pundt, A.; Kirchheim, R.; Molen, S. J. V. D.; Kooij, E. S.; Kerssemakers, J.; Griessen, R.; Harms, H.; Geyer, U. Stress Development in Thin Yttrium Films on Hard Substrates during Hydrogen Loading. *J. Appl. Phys.* **2003**, *93* (11), 8958−8965.

https://doi.org/10.1021/acsphotonics.1c00393
ACS Photonics 2021, 8, 1810−1816